Effects of surface wettability and liquid viscosity on the dynamic wetting of individual drops

Longquan Chen and Elmar Bonaccurso*

Center of Smart Interfaces, Technische Universität Darmstadt, Alarich-Weiss-Strasse 10, 64287 Darmstadt, Germany

(Received 15 August 2013; revised manuscript received 11 December 2013; published 4 August 2014)

In this paper, we experimentally investigated the dynamic spreading of liquid drops on solid surfaces. Drop of glycerol water mixtures and pure water that have comparable surface tensions (62.3–72.8 mN/m) but different viscosities (1.0–60.1 cP) were used. The size of the drops was 0.5–1.2 mm. Solid surfaces with different lyophilic and lyophobic coatings (equilibrium contact angle θ_{eq} of 0°–112°) were used to study the effect of surface wettability. We show that surface wettability and liquid viscosity influence wetting dynamics and affect either the coefficient or the exponent of the power law that describes the growth of the wetting radius. In the early inertial wetting regime, the coefficient of the wetting power law increases with surface wettability but decreases with liquid viscosity. In contrast, the exponent of the power law does only depend on surface wettability as also reported in literature. It was further found that surface wettability does not affect the duration of inertial wetting, whereas the viscosity of the liquid does. For low viscosity liquids, the duration of inertial wetting corresponds to the time of capillary wave propagation, which can be determined by Lamb's drop oscillation model for inviscid liquids. For relatively high viscosity liquids, the inertial wetting time increases with liquid viscosity, which may due to the viscous damping of the surface capillary waves. Furthermore, we observed a viscous wetting regime only on surfaces with an equilibrium contact angle θ_{eq} smaller than a critical angle θ_c depending on viscosity. A scaling analysis based on Navier-Stokes equations is presented at the end, and the predicted θ_c matches with experimental observations without any additional fitting parameters.

DOI: 10.1103/PhysRevE.90.022401 PACS number(s): 68.08.Bc, 47.55.dr, 47.55.df, 47.55.np

I. INTRODUCTION

When a liquid drop is placed on a solid substrate, the unbalanced interfacial tensions γ, γ_{LS}, and γ_{SV} at the liquid-solid-vapor contact line cause it to spread towards its equilibrium state. This simple phenomenon is key for many industrial applications, and it has been a research topic for scientists and engineers for more than two centuries [1–7]. Benefitting also from the development of high speed video cameras, the entire spreading process became accessible in recent years, and experimental investigations especially about the early wetting regimes have been boosted by this technological progress [1,6,8–22].

Just after the drop contacts the substrate, inertia of the drop resists the capillary driven spreading, and the spreading radius r grows with spreading time t according to a power law $r = Ct^{0.5}$ independent of surface wettability for liquids with low viscosity [11,13,19]; C is a coefficient. When $t \gtrsim 0.1$ ms, spreading is still inertial for low viscosity liquids, but the radius grows as $r = C't^{\alpha}$ [8,9,12,14,17,18] with C' as another coefficient. The exponent α only depends on surface wettability, i.e., on the equilibrium contact angle θ_{eq}, and $\alpha \propto \sqrt{F(\theta_{eq}) + \cos\theta_{eq}}$ with $F(\theta_{eq})$ as an unknown function [9]. The duration of this second stage is usually defined by the characteristic inertial time $\tau_i \approx \sqrt{\frac{\rho R^3}{\gamma}}$ [8,9,12,14,17,19]; ρ and R are the density and radius of the drop.

On very lyophilic ($\theta_{eq} \ll 60^\circ$ or 1 rad) or complete wetting surfaces ($\theta_{eq} = 0^\circ$), a third wetting stage was observed in most experimental investigations [6,10,21,22]. As spreading proceeds, the spreading velocity slows down, and viscous friction inside the drop becomes the main source opposing capillarity as the inertial forces decrease. In the case of a small drop with a size smaller than the capillary length $\lambda_c = \sqrt{\frac{\gamma}{\rho g}}$, a time dependence of the spreading radius $r \sim R(\frac{\gamma}{\mu R})^{1/10} t^{1/10}$ was theoretically derived with the assumption of volume conservation [1,15,16]. Here, g is the acceleration due to gravity, and μ is the dynamic viscosity of the liquid. This wetting law is also called *Tanner's law* and was experimentally validated by numerous studies [6,10,21,22]. For drops with $R > \lambda_c$, the effect of gravity as a driving force for spreading becomes more relevant, and drop spreading follows another power law $r \sim R(\frac{R\rho g}{\mu})^{1/8} t^{1/8}$ [10,23]. On partially wetting substrates, spreading drops approach equilibrium with an exponential law [15,24].

In literature, much effort was devoted to investigate the influence of wettability [8,9,11,13,19,21], surface patterns [10,14,25,26], softness [11,12,27], or even surface solubility [17] on early inertial wetting dynamics. In contrast, the effects of viscosity on spreading received little attention up to now [28]. Blake and co-workers investigated the impinging of liquid curtains with different viscosities onto a moving solid, and they found that the dynamic wetting was also influenced by the hydrodynamic flow away from the contact line [29,30]. For spontaneous wetting, one would expect that highly viscous liquids spread slower than low viscous liquids. Thus, a natural question arising is whether viscosity influences the early wetting dynamics, and if it does, how and to which extent? On the other hand, the viscous wetting regime was mostly reported on strongly lyophilic or complete wetting surfaces [6,8,10,22,31]. Most recently, McHale and co-workers investigated dielectrowetting on complete and partial wetting surfaces with spreading dominated by viscous dissipation [24]. It is, however, still not clear if the viscous

*Author to whom correspondence should be addressed: elmar.bonaccurso@eads.net; Present address: Airbus Group Innovations, 81663 Munich, Germany.

TABLE I. Equilibrium contact angles of the liquids listed in Table II on substrates modified by different types of coatings.

Surfaces	$\theta_{eq}/\theta_{ad}/\theta_{re}$ (°)				
wt % glycerol	0	40	60	75	80
Silicon dioxide	–/–/–[a]	–/–/–	–/–/–	–/–/–	–/–/–
Triethoxysilyl butyraldehyde	41±4/71±3/30±2	41±6/61±2/19±3	34±5/61±2/16±2	40±7/58±2/14±2	41±5/56±3/11±3
3-aminopropyltriethoxysilane	63±5/88±2/46±3	56±5/57±2/30±1	57±9/71±3/75±3	54±3/64±2/13±1	60±9/71±3/8±1
1,1,1,3,3,3-hexamethyldisilazane	92±5/106±2/83±3	85±3/98±3/74±2	92±6/104±3/75±3	87±8/107±6/79±3	104±5/114±3/72±2
1H,1H,2H,2H-perfluorodecyltriethoxysilane	112±4/116±3/100±2	105±6/113±4/75±2	107±5/119±2/75±3	109±9/115±3/80±2	110±6/119±2/75±1

[a]Contact angles were so small that they could not be measured accurately; value is of order of experimental error.

wetting stage arises during spontaneous spreading of drops on partial wetting surfaces.

In this paper, we thus experimentally investigated the dynamic wetting of surfaces with different wettabilities by liquids with different viscosities. We focused on the wetting dynamics beyond approximately 0.1 ms and found that it was influenced by both surface wettability and liquid viscosity. In the inertial stage, the coefficient of the power law decreased with equilibrium contact angle and liquid viscosity, but the exponent was only dependent on surface wettability as reported earlier in literature. We observed viscous wetting only on surfaces with an equilibrium contact angle smaller than a critical value, which depended also on the liquid viscosity. We propose a scaling analysis for explaining our observations.

II. EXPERIMENT

A. Surfaces and liquids

We prepared surfaces with different wettabilities using a variety of coatings (Table I). Smooth glass slides were cleaned in acetone (p.a., Sigma-Aldrich, Germany) and then ethanol (p.a., Sigma-Aldrich, Germany) in an ultrasonic bath for 5 min each. After rinsing in Milli-Q water, the surfaces were dried with purified nitrogen. By treatment with oxygen plasma (Femto, Diener Electronic GmbH, Germany) for 5 min, we obtained complete wetting surfaces (surface 1). The other two lyophilic surfaces (surfaces 2 and 3) were prepared following a standard silanization procedure [2]. The two lyophobic surfaces (surfaces 4 and 5) were fabricated by silanization of oxygen plasma treated glass slides in vapor phase in a desiccator at 100 °C overnight.

We performed wetting experiments with pure water and with four glycerol water mixtures under room temperature of 22 ± 2 °C and relative humidity of $45\% \pm 3\%$. These liquids have a slightly different surface tension (the difference is less than 17%) but a remarkably different viscosity (the maximum viscosity is 60 times larger than the viscosity of pure water, see Table II). During the experiments (~200 ms), the change in droplet volume was less than 1%. Therefore, both the change in surface tension and the viscosity due to the hygroscopic property of glycerol or due to drop evaporation during spreading can be neglected.

The contact angles of all liquids on all surfaces were directly obtained from the recorded images for each experiment (Table I). Advancing and receding contact angles (Table I) were measured with a commercial goniometer (Krüss, DSA 100, Germany).

B. Observation of the wetting process

Pendant drops were generated and approached the substrates using a syringe pump. The speed of the approaching drop just before contact is ~0.1 mm/s, which is much smaller than the early wetting speed (~0.5 m/s), and thus the influence of the kinetic energy of the drop on spreading could be neglected. We studied spreading experiments of drops with radii R between 0.5 and 1.2 mm. These sizes are all smaller than the respective capillary length (Table II). Needle and substrates were grounded to prevent the influence of electrostatics on spreading [11,14]. The spreading process was recorded with a high speed camera (FASTCAM SA-1, Photron, Inc.) with recording rates of 10 000–54 000 frames per second. Each experiment was repeated at least five times with fresh surfaces.

C. Data analysis

The spreading radius r was extracted from the recorded movies with an *ad hoc* developed MATLAB (Math Works, Inc.) algorithm. Since the early wetting dynamics is dominated by inertia, we used the Pearson product-moment correlation

TABLE II. Physical properties of the liquids and corresponding capillary length and characteristic viscous speed.

Liquids	ρ (kg/m^3) [32]	γ (mN/m) [33]	μ (mPa s) [34]	λ_c (mm)	γ/μ (mm/ms)
Water	998.2	72.8	1.00	2.7	72.8
40 wt % glycerol	1099.3	69.2	3.7	2.5	18.7
60 wt % glycerol	1153.8	67.2	10.7	2.4	6.3
75 wt % glycerol	1194.9	63.5	35.5	2.3	1.8
80 wt % glycerol	1208.5	62.3	60.1	2.3	1.0

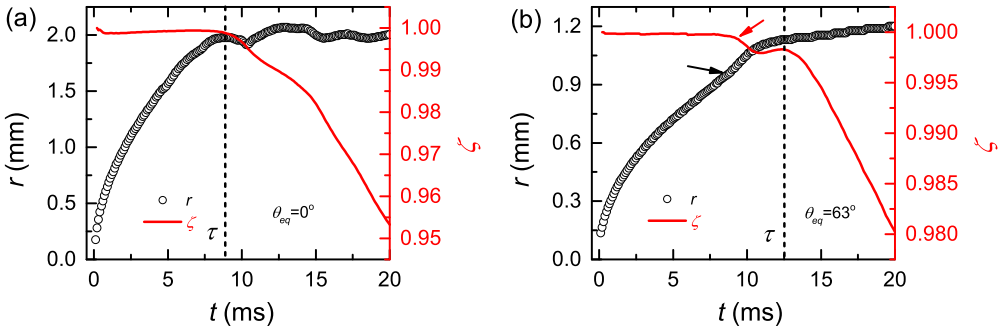

FIG. 1. (Color online) Spreading radius r and linear correlation coefficient ζ between $\log r$ and $\log t$ as a function of time t. (a) The substrate is silicon oxide, and the drop is water. The corresponding equilibrium contact angle is 0°. (b) The substrate is 3-aminopropyltriethoxysilane coated silicon, and the liquid is a 75% glycerol water mixture. The corresponding equilibrium contact angle is 63°. The black and red arrows show the influence of drop detachment from the needle on the spreading radius and on the linear correlation coefficient, respectively. The drop radius is always 0.9 mm.

coefficient ζ to check the power law relationship between r and t,

$$\zeta = -\frac{\sum_{i=1}^{n}(r_i' - \bar{r}')(t_i' - \bar{t}')}{\sqrt{\sum_{i=1}^{n}(r_i' - \bar{r}')^2}\sqrt{\sum_{i=1}^{n}(t_i' - \bar{t}')^2}}, \quad r' = \log r,$$

$$t' = \log t, \quad \bar{r}' = \frac{1}{n}\sum_{i=1}^{n} r_i', \quad \bar{t}' = \frac{1}{n}\sum_{i=1}^{n} t_i'.$$

ζ has a value between -1 and 1. ζ equaling 1 or -1 corresponds to a very good linear relationship between $\log r$ and $\log t$, i.e., a very strong power law relationship between r and t. Figure 1 shows the spreading radius r and the corresponding ζ as a function of time t for a water drop spreading on a complete wetting surface and a 75% glycerol water drop spreading on a 3-aminopropyltriethoxysilane coated silicon surface, respectively. ζ is $\sim$1 when t is smaller than a characteristic time $\tau \approx 9$ ms for water and $\tau \approx 12$ ms for a 75% glycerol water mixture, beyond which ζ starts to diverge. This indicates that wetting at $t \leqslant \tau$ follows a power law. We thus fitted these data with a power law using the least squares method (LSM). It is noted that there is a kink for r near τ on relatively lyophobic surfaces [Figs. 1(b) and 3(a)], which is due to the drop detaching from the needle. This caused slight variations and oscillations in ζ, but a strong power law relationship between r and t still exists.

III. RESULTS AND DISCUSSION

Figures 2(a) and 2(b) show the effects of surface wettability on drop spreading. When drops touch the surfaces, the liquid on the surface spreads out spontaneously, whereas the liquid further away does not yet flow. Similar to other studies [8,9,12], capillary wave propagation along the surface was observed as drop spreading started. The spreading was faster on lyophilic surfaces [Fig. 2(a)] and slower on lyophobic surfaces [Fig. 2(b)]. The spreading on complete wetting surfaces was so fast that the drop was first disrupted into two parts ($\sim$5 ms), before recoalescing ($\sim$10 ms). In contrast, the drop was transferred as a whole to the partial wetting surfaces after several milliseconds (depending on drop size), even if a distortion of the drop still occurred. When the drop is finally completely transferred to the surface and detached from the needle (7 to 8 ms), the energy stored in the drop deformation is released and causes strong oscillations (7 to 8 ms in Fig. 1 and 10–50 ms in Figs. 2(a) and 2(b). We performed similar spreading experiments by approaching the surfaces from the top to drops sitting on superamphiphobic surfaces as suggested by Biance *et al.* [8]. We did not observe any major differences between the two types of experiments. On complete wetting surfaces, drops went on spreading with a gradual decreasing speed until the contact angle approached zero. On partial wetting surfaces, drops stopped spreading and reached equilibrium only after the oscillations stopped.

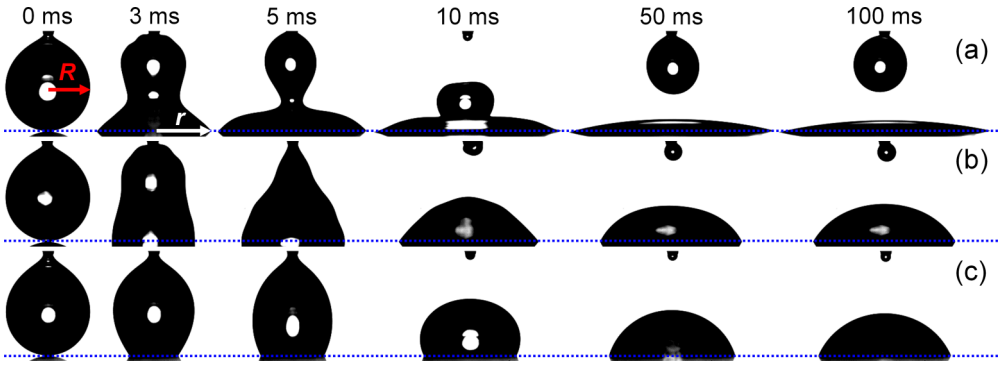

FIG. 2. (Color online) (a) Water drop spreading on a complete wetting surface ($\theta_{eq} \approx 0°$). (b) Water drop spreading on a partial wetting surface ($\theta_{eq} \approx 60°$). (c)An 80% glycerol water drop spreading on the same surface as in (b). The initial drop radius was always 0.9 mm.

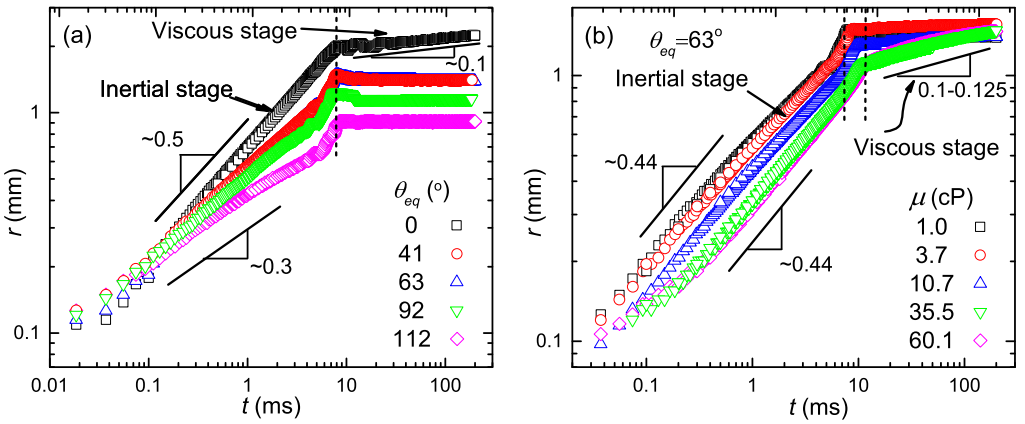

FIG. 3. (Color online) (a) Log-log plot of the spreading radius r as a function of time t of water drops on five surfaces and (b) of drops of different liquids on a partial wetting surface ($\theta_{eq} = 63^\circ$). The initial drop radius was always ~0.9 mm.

Figures 2(b) and 2(c) show the effects of liquid viscosity on drop spreading on a partial wetting surface. Spreading was faster for low viscosity liquids than that for highly viscous liquids. For highly viscous liquids, after complete drop transfer onto the substrate spreading just slowed down [~10 ms in Fig. 2(c)] but did not stop completely. Therefore, a slower wetting stage was also observed on partial wetting surfaces. Moreover, the oscillation of highly viscous liquids was weaker than that of liquids with a lower viscosity.

Figure 3(a) shows the log-log plot of r vs t of water drops spreading on five surfaces with different wettabilities. The wetting for $t \lesssim 9$ ms followed the power law $r = C't^{\alpha}$. The slope α increased from ~0.3 to ~0.5, whereas θ_{eq} decreased from ~112° to ~0°, which was consistent with previous studies [8,9,12,17] and a most recent molecular dynamics simulations study [35]. The kink at 7 to 8 ms in Fig. 3 is a signature of drop detachment from the needle. Before the kink spreading was briefly slowed down, and after the kink it was accelerated due to an additional release of energy previously stored in the drop deformation. The acceleration of the spreading is stronger on lyophobic surfaces than that on lyophilic surfaces [Fig. 3(a)]. However, this caused only a slight change in the linear correlation coefficient and did not affect the analysis (a critical time τ still exists as shown in Fig. 1). On complete wetting surfaces only a subsequent slower wetting stage with an average spreading speed of ~0.002 m/s was observed for $t \gtrsim 9$ ms. The power law fitting of the data resulted in a slope of ~0.1, indicating that spreading was dominated by viscous dissipation. No such slow wetting stages were found on partial wetting surfaces, and drops were simply oscillating around the equilibrium state with a pinned contact line for $t \gtrsim 9$ ms [Fig. 3(a)]. In the late stage of dynamic wetting on lyophilic surfaces or in dielectrowetting experiments [24] it was found that after the wetting stage characterized by the drop radius growing with a power law, the drop radius approached its equilibrium value with a logarithmic law. However, we did not observe logarithmic wetting dynamics on any lyophobic surfaces within ~200 ms after drop deposition, i.e., the time range of our observations.

Figure 3(b) shows the effects of viscosity on dynamic wetting of a partial wetting surface ($\theta_{eq} = 63^\circ$). The spreading also followed a power law, and it was slower for liquids with higher viscosity, i.e., C' decreased with μ, and τ slightly increased from ~9 to ~13 ms as μ increased from 1 to 60.1 cP. $\alpha \approx 0.44$ for all liquids since θ_{eq} was similar. For liquids with $\mu < 35.5$ cP no viscous wetting was observed, and drops reached the equilibrium contact radii when $t > \tau$. For liquids with $\mu \gtrsim 35.5$ cP the drops continued spreading when $t > \tau$, according to a power law with an exponent between 0.1 and 0.125. Exponents larger than 0.1 are due to gravity effects. In fact, even if the sessile drops were still spherical [between 50 and 100 ms, Fig. 2(c)], their sizes were close to the capillary length (Table II), and the more viscous drops having smaller capillary lengths. Thus, gravity influenced drop spreading, the influence increasing with decreasing capillary length and increasing viscosity (Fig. 4). In conclusion, we found that surface wettability and liquid viscosity influenced wetting dynamics of individual drops spreading on solid surfaces.

We further like to point out that the viscous wetting stage we describe above is different from the viscous stage observed during the coalescence of two droplets. In the very early stage of drop coalescence (typically, $t < 0.7$ ns), the flow is driven by a highly curved meniscus and is resisted by viscous forces and has a velocity on the order of the characteristic viscous speed (Table II). Eggers *et al.* predicted that the

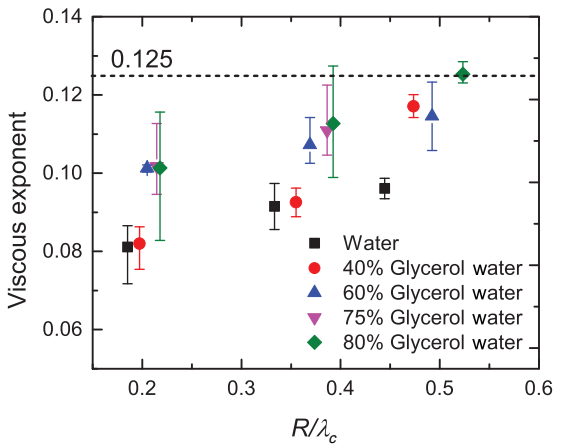

FIG. 4. (Color online) The viscous exponent of various liquids as a function of the normalized radius R/λ_c for all experiments showing the viscous wetting stage (full symbols in Fig. 9).

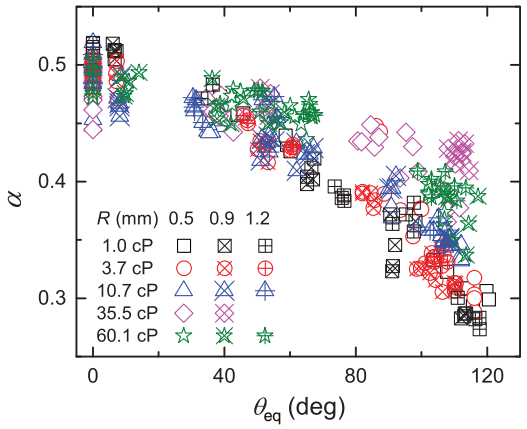

FIG. 5. (Color online) α as a function of θ_{eq} for drops with five different viscosities and three sizes.

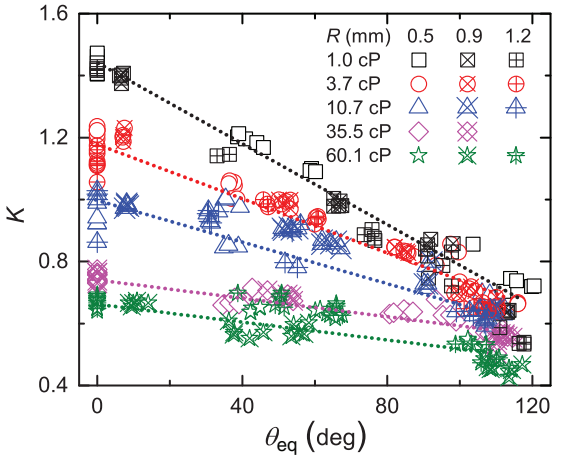

FIG. 6. (Color online) Normalized inertial coefficient K as a function of θ_{eq} and μ. The dotted lines are guides for the eye.

dynamics follows a logarithmic law [36], which recently was experimentally confirmed by Paulsen *et al.* [37]. In contrast, the viscous wetting stage we observe appears much later ($t \gtrsim 9$ ms), and its characteristic speed is much slower than the characteristic viscous speed of drop coalescence.

A. Inertial wetting

We fitted our experimental data for $t \lesssim \tau$ with a power law $r = C't^{\alpha}$ using the LSM. For inertial wetting, the exponent of the power law was only dependent on θ_{eq} [8,9,12]. Figure 5 summarizes α's of drops with different sizes and viscosity spreading on different wettable surfaces. α's laid between 0.3 and 0.5 and decreased with θ_{eq} regardless of drop viscosity, density, or size. This is consistent with theoretical predictions [9,11] and experimental results [8,9,11,12,17] from literature. Recently, Legendre and Maglio numerically calculated that if the early wetting was dominated by viscous dissipation, the spreading should follow a power law with $\alpha = 2/3$ [38]. However, in our experiments we found that the maximum α for all liquids was 0.5 and that α was only dependent on θ_{eq}. So it seems to confirm that the early wetting dynamics of individual spreading drops is dominated by inertia but not by viscous dissipation.

With the same surface and liquid, C' was larger for larger drops [Fig. 3(b)], which was also found by Bird *et al.* [9]. For a specific drop size, we found C' was smaller for more viscous liquids. Moreover, with increasing θ_{eq}, C' decreased. Generally, we observed that C' was determined by drop size, liquid viscosity, and surface wettability, i.e., $C' = C'(R,\mu,\theta_{eq})$.

In Fig. 6, we further show the normalized inertial coefficient $K = \frac{C'\tau_i^{\alpha}}{R}$ from the normalized power law fitting $\frac{r}{R} = K(\frac{t}{\tau_i})^{\alpha}$ as a function of θ_{eq} and μ for three different drop sizes. The coefficient for different drop sizes collapsed into five curves, each of which corresponds to one viscosity. These curves decrease with μ and θ_{eq}. This is yet one more evidence that the early wetting dynamics is dominated by inertia, but it is also influenced by surface wettability and liquid viscosity.

In the following we try to explain the influence of surface wettability and liquid viscosity on the inertial wetting coefficient. In the paper by Bird *et al.*, the authors proposed a scaling analysis of inertial wetting based on energy conservation [9]. They considered that the change in surface energy during spreading was transferred into the kinetic energy of the moving drop within a self-similar velocity field over a length scale $l_v \propto (\frac{\gamma t^2}{\rho})^{1/3}$. In other words, the effective mass of the moving drop scales as ρl_v^3. Thus, one possibility is that surface wettability and liquid viscosity influence the effective mass of spreading drops, i.e., the extension of the velocity field l_v.

In order to estimate the extension of the velocity field, we tracked the profiles of the spreading drops. As illustrated in Fig. 7(a), we superposed the liquid-air interfaces (contours) of drops at times t and $t - \Delta t$. We traced a (horizontal) line between the two crossing points of the contours. This line is at a distance l from the solid surface. Between this line and the solid surface drops spread out during Δt, whereas above the line drops moved in the reverse direction on lyophilic surfaces or oscillated slightly on lyophobic surfaces due to capillary waves as shown in Fig. 7(b). Therefore, l could be treated as a length scale characterizing the velocity field at time t [Fig. 7(a)]. However, Δt should not be too small to still allow identifying the change in the drop contour. The minimum time step that we used to extract l from our experimental data was 0.1 ms. As spreading went on, l grew with time, and the growth depended on surface wettability and liquid viscosity [Fig. 7(b)].

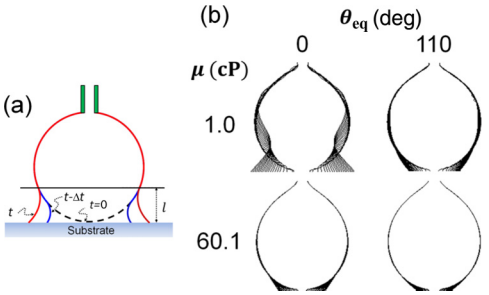

FIG. 7. (Color online) (a) Schematics of the change in the liquid-air interface (contour) of the drop during spreading. (b) Contours of the droplets of two liquids spreading on two wetting surfaces. The initial radius of all drops was ~0.9 mm. The interval between two profiles is 0.1 ms.

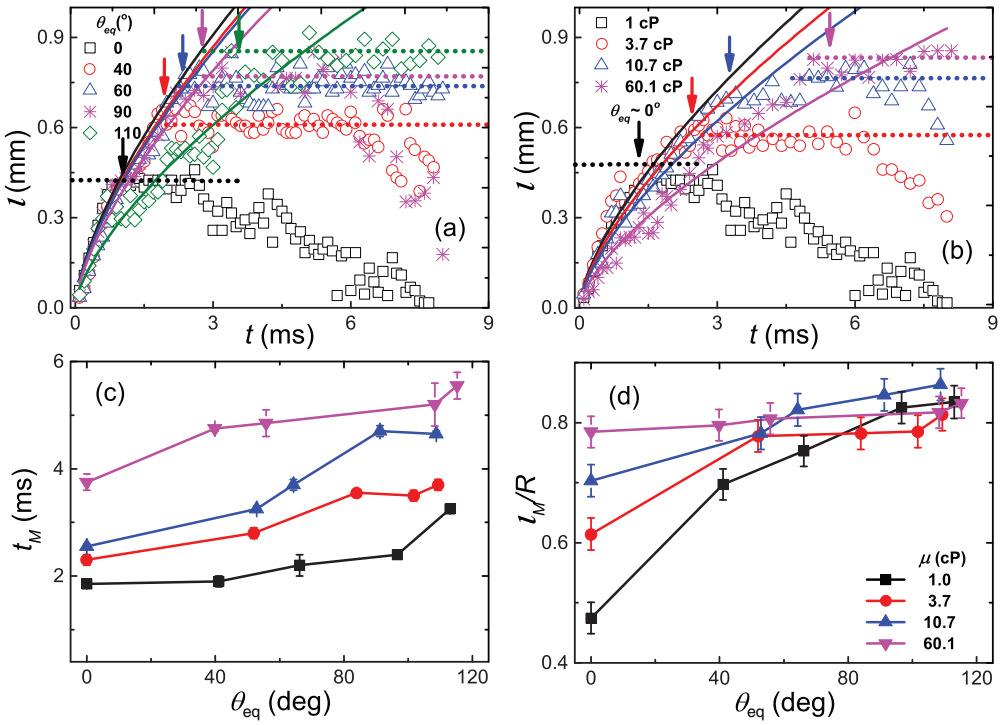

FIG. 8. (Color online) (a) Extension of the velocity field l as a function of spreading time t for water on differently wettable surfaces. (b) Extension of the velocity field l as a function of spreading time t for different liquids on a complete wetting surface. The dotted color lines in (a) and (b) indicate the maximum extension l_M, and the solid lines are fits with $l = k(\frac{\gamma t^2}{\rho})^{1/3}$. (c) Time t_M needed to reach the maximum extension and (d) maximum normalized extension l_M/R as a function of θ_{eq} and μ. The initial radius of all drops was ~0.9 mm.

Figure 8(a) shows l vs t for a 0.9-mm-radius water drop spreading on different surfaces. We found that l initially grew with t according to $l = k(\frac{\gamma t^2}{\rho})^{1/3}$ on all surfaces. Similar trends were also observed for the other four liquids with different viscosities. This finding confirmed the assumption by Bird *et al.* that the liquid adjacent to the solid surface flows within a self-similar velocity field [9]. However, the process describing the developing velocity field is related to surface wettability and liquid viscosity, i.e., $k = k(\theta_{eq}, \mu)$. As shown in Figs. 8(a) and 8(b), k decreased with θ_{eq} and μ. After a characteristic time t_M, which was always smaller than τ, l reached a maximum extension l_M and then kept nearly constant until the end of inertial wetting. This is indicated by arrows. Also t_M and l_M were dependent on θ_{eq} and μ as summarized in Figs. 8(c) and 8(d). For the same liquid, t_M and l_M increased with θ_{eq}, i.e., it took longer to reach the maximum extension of the velocity field on lyophobic surfaces, and the corresponding l_M was larger. On similar surfaces, t_M and l_M also increased with μ [Figs. 8(c) and 8(d)]. We could therefore conclude that the velocity field in the spreading drop developed in a self-similar way that was controlled by surface wettability and liquid viscosity.

As pointed out above, θ_{eq} and μ influence the development of the self-similar velocity field during drop spreading, and so they eventually influence the power law of inertial wetting. However, it is difficult to take this effect into account in the power law derivation. Instead of a quantitative analysis, we give a qualitative explanation here. For spreading with a large t_M and l_M, i.e., for wetting with highly viscous liquids or on lyophobic surfaces the effective mass of the spreading drop is large, and hence the spreading velocity is slow as the driving capillary force is similar during inertial wetting. Since the early wetting dynamics is dominated by inertia and the inertial exponent α is only dependent on θ_{eq}, a smaller coefficient C' or K can reasonably be expected. This argument is consistent with our observation in Figs. 3 and 6.

Most recently, Carlson and co-workers considered the influence of surface wettability and liquid viscosity on dynamic wetting by introducing additional energy dissipation terms, such as contact line friction due to molecular process, viscous dissipation in the liquid, and a diffusive dissipation [39–41]. However, these contributions are hard to be directly integrated into the derivation of the power law of inertial wetting.

B. Inertial wetting time

The inertial wetting lasts only from a few to a few tens of milliseconds, depending on drop size. Then, the drop reaches equilibrium or crosses over into the slower viscous wetting regime. Figure 9(a) shows the inertial time τ as a function of θ_{eq} for four different liquids. Similar to other studies [8,9,12], we found that the inertial time τ was independent of θ_{eq} and was always larger than the characteristic inertial time $\tau_i = \sqrt{\frac{\rho R^3}{\gamma}}$. Moreover, we also observed that τ was larger for more viscous liquids. Biance *et al.* suggested that the inertial wetting stops at the crossover from the inertial to the viscous wetting regime [8]. They found that inertial wetting was shorter for higher viscous liquids, which is—however—in contrast to our experimental results here. Another model to explain the duration of inertial wetting was proposed by Bird

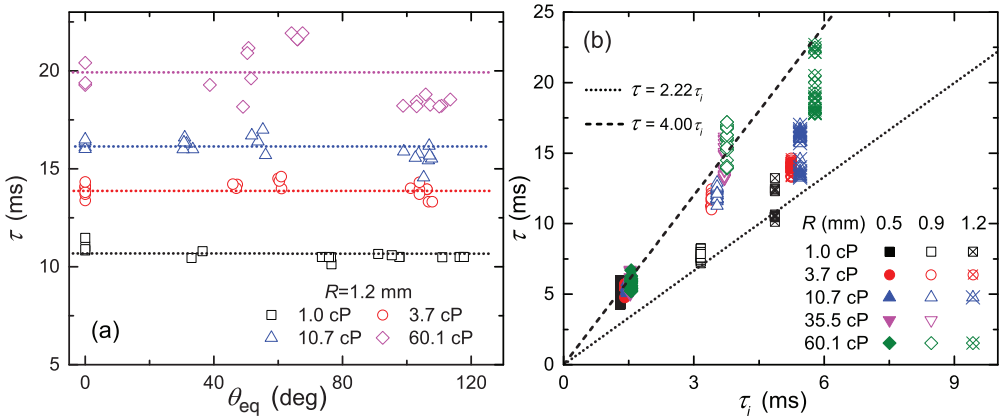

FIG. 9. (Color online) (a) Inertial wetting time τ as a function of θ_{eq} for four liquids with different viscosities on completely wetting surfaces. The drop radius is ~1.2 mm. (b) τ as a function of τ_i for various liquids and different drop sizes.

et al. [9]: inertial wetting lasted as long as the propagation time of the capillary wave along the drop. Based on the vibration model of suspended drops proposed by Lamb [42], Chen and co-workers [11,12] found the actual inertial time was $\tau \approx 2.22\tau_i$ for low viscosity liquids. Figure 9(b) summarizes the actual inertial wetting time τ as a function of τ_i for various drop sizes and liquids. τ increased linearly with τ_i and was very close to the theoretical prediction for low viscosity liquids, such as water. For more viscous liquids, τ was larger than τ_i and increased with μ. For liquids with $\mu \gtrsim 35.5$cP, $\tau \approx 4.0\tau_i$. We ascribe this to the viscous damping of the capillary wave. In Lamb's model [42], the vibrating drop was treated as a spring since the liquid was considered inviscid. For the vibration of relatively viscous drops, viscous damping will cause a decrease in the vibration frequency [43] and hence will result in $\tau > 2.22\tau_i$. For the vibration of extremely viscous drops, the oscillation frequency is scaled with the relaxation time $f \sim \frac{\gamma}{\mu R}$ [43].

C. Viscous wetting

When spreading proceeds, the inertial resistance lessens, and the viscous dissipation in the drop becomes dominant [8,9]. However, we only observed viscous wetting on surfaces with an equilibrium contact angle smaller than a critical value θ_c, characteristic for each liquid. As shown in the wetting phase diagram (Fig. 10), θ_c increased with μ. Since the Reynolds number Re compares inertial with viscous forces, we analyzed Re during the spreading. Due to the symmetry of the drop spreading process, we applied the two dimensional Navier-Stokes equations with the incompressibility condition,

$$\rho\left(u\frac{\partial u}{\partial x}+v\frac{\partial u}{\partial y}\right)=-\frac{\partial p}{\partial x}+\mu\left(\frac{\partial^2 u}{\partial x^2}+\frac{\partial^2 u}{\partial y^2}\right), \quad (1)$$

$$\rho\left(u\frac{\partial v}{\partial x}+v\frac{\partial v}{\partial y}\right)=-\frac{\partial p}{\partial y}+\mu\left(\frac{\partial^2 v}{\partial x^2}+\frac{\partial^2 v}{\partial y^2}\right), \quad (2)$$

$$\frac{\partial u}{\partial x}+\frac{\partial v}{\partial y}=0. \quad (3)$$

u and v are the velocity components in the tangential and the vertical directions, respectively, and p is the pressure. The terms on the left-hand side in Eqs. (1) and (2) are the inertial terms, and the last terms on the right-hand side are the viscous terms. Let U^* and V^* be characteristic velocities, and R^* and H^* be the characteristic length of the contact radius and height of the spreading drop. From the nondimensional form of Eq. (3), we obtain

$$V^*=\varepsilon U^*, \quad \varepsilon=\frac{H^*}{R^*}. \quad (4)$$

With the above expression, we can estimate the inertial and viscous terms in Eq. (1),

$$\rho u\frac{\partial u}{\partial x}\sim\rho v\frac{\partial u}{\partial y}\sim\frac{\rho U^{*2}}{R^*}, \quad (5)$$

$$\mu\frac{\partial^2 u}{\partial x^2}\sim\frac{\mu U^*}{R^{*2}}, \quad \mu\frac{\partial^2 u}{\partial y^2}\sim\frac{\mu U^*}{\varepsilon^2 R^{*2}}. \quad (6)$$

In the inertial stage, $R^* \sim H^* \sim R$ and $\mu\frac{\partial^2 u}{\partial x^2}\sim\mu\frac{\partial^2 u}{\partial y^2}$. In the viscous stage, the drop height is always much smaller than the contact radius [1,15,16], i.e., $\varepsilon \ll 1$, which leads

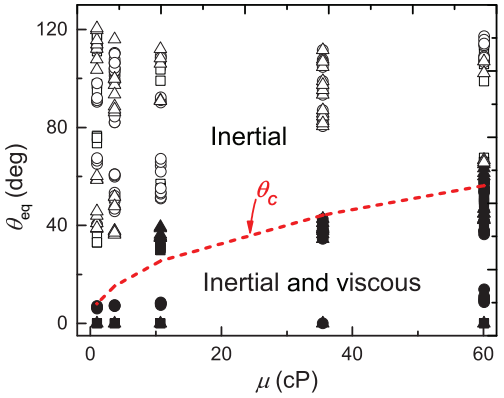

FIG. 10. (Color online) Wetting phase diagram of drop spreading on solid surfaces as a function of liquid viscosity μ and equilibrium contact angle θ_{eq}. Symbol shapes indicate different drop sizes R: (■, □) 1.2 mm, (●, ○) 0.9 mm, and (▲, △) 0.5 mm. The open symbols tell that one wetting stage only (inertial) was observed, and the closed symbols tell that two stages (inertial and viscous) were observed. The red dashed line is a plot of Eq. (9) with liquid properties as in experiments and no free fitting parameters.

to $\mu\frac{\partial^2 u}{\partial x^2} \ll \mu\frac{\partial^2 u}{\partial y^2}$. Thus, the Reynolds number in both wetting stages takes the same form

$$\mathrm{Re} \sim \frac{\rho u\frac{\partial u}{\partial x}}{\mu\frac{\partial^2 u}{\partial y^2}} \sim \varepsilon^2\frac{\rho U^* R^*}{\mu}. \quad (7)$$

At the end of the inertial regime $R^* \sim R$ and the characteristic tangential velocity scales as $U^* \sim \sqrt{\frac{\gamma}{\rho R}}$. The viscous wetting regime can only be observed when the viscous forces dominate over the inertial forces,

$$\mathrm{Re} \sim \varepsilon^2\frac{\rho U^* R^*}{\mu} \sim \varepsilon^2\frac{\rho}{\mu}\sqrt{\frac{\gamma R}{\rho}} < 1. \quad (8)$$

Solving Eq. (8), we find that a viscous spreading drop should have a shape with $\varepsilon < \frac{\mu^{1/2}}{(\rho R\gamma)^{1/4}}$. Making the—reasonable—assumption that the shape of the drop is hemispherical and the contact angle is close to θ_{eq}, we finally obtain the criteria for observing viscous wetting depending on surface wettability and viscosity,

$$\theta_{\mathrm{eq}} < \theta_c = \sin^{-1}\frac{2\varepsilon_c}{1+\varepsilon_c^2}, \quad (9)$$

with $\varepsilon_c = \frac{\mu^{1/2}}{(\rho R\gamma)^{1/4}}$.

As shown in Fig. 10, the critical θ_c predicted by Eq. (9) (red dashed line) matches our experimental observations very well without any need for additional fitting parameters.

IV. SUMMARY

To summarize, we found that surface wettability and liquid viscosity influence the wetting dynamics of individual droplets spreading on solid surfaces. First, during the inertial wetting regime, surface wettability and liquid viscosity influenced the inertial power law coefficient, whereas the inertial power law exponent only depended on surface wettability. This is because the effective mass of the spreading drop is influenced by surface wettability and liquid viscosity. The duration of the inertial wetting regime is longer for more viscous liquids due to the viscous damping of drop oscillations. Second, we observed viscous wetting only on surfaces with θ_{eq} smaller than a critical value θ_c, which depended on the liquid properties and specifically on the dynamic viscosity. Upon a scaling analysis based on the Navier-Stokes equations, we proposed an expression for θ_c that matched the experimental observations without any free fitting parameters.

ACKNOWLEDGMENTS

We acknowledge useful discussions with X. Wang, G. K. Auernhammer, and H.-J. Butt. This research was supported by the German Research Foundation (DFG) within the Cluster of Excellence 259 "Smart Interfaces—Understanding and Designing Fluid Boundaries."

[1] P. G. de Gennes, C. R. Acad. Sci., Ser. II: Mec., Phys., Chim., Sci. Terre Univers **298**, 111 (1984).
[2] P. G. de Gennes, F. Brochard-Wyart, and D. Quere, *Capillarity and Wetting Phenomena* (Springer, New York, 2004).
[3] P. S. de Laplace, *Traité de Mécanique Céleste* (Courcier, Paris, 1805).
[4] A. Einstein, Ann. Phys. (Leipzig) **309**, 513 (1901).
[5] E. Schrödinger, Ann. Phys. (NY) **351**, 413 (1915).
[6] L. H. Tanner, J. Phys. D: Appl. Phys. **12**, 1473 (1979).
[7] T. Young, Philos. Trans. R. Soc. London **95**, 65 (1805).
[8] A.-L. Biance, C. Clanet, and D. Quéré, Phys. Rev. E **69**, 016301 (2004).
[9] J. C. Bird, S. Mandre, and H. A. Stone, Phys. Rev. Lett. **100**, 234501 (2008).
[10] A. M. Cazabat and M. A. C. Stuart, J. Phys. Chem. **90**, 5845 (1986).
[11] L. Q. Chen, E. Bonaccurso, and M. E. R. Shanahan, Langmuir **29**, 1893 (2013).
[12] L. Q. Chen, G. K. Auernhammer, and E. Bonaccurso, Soft Matter **7**, 9084 (2011).
[13] L. Q. Chen, L. O. Heim, D. S. Golovko, and E. Bonaccurso, Appl. Phys. Lett. **101**, 3 (2012).
[14] L. Courbin, J. C. Bird, M. Reyssat, and H. A. Stone, J. Phys.: Condens. Matter **21**, 464127 (2009).
[15] P. G. de Gennes, Rev. Mod. Phys. **57**, 827 (1985).
[16] C. Huh and L. E. Scriven, J. Colloid Interface Sci. **35**, 85 (1971).
[17] P. Muralidhar, E. Bonaccurso, G. K. Auernhammer, and H. J. Butt, Colloid Polym. Sci. **289**, 1609 (2011).
[18] O. A. Soboleva, E. A. Raud, and B. D. Summ, Kolloidn. Zh. **53**, 1106 (1991).
[19] K. G. Winkels, J. H. Weijs, A. Eddi, and J. H. Snoeijer, Phys. Rev. E **85**, 055301(R) (2012).
[20] L. Q. Chen, C. L. Li, N. F. A. van der Vegt, G. K. Auernhammer, and E. Bonaccurso, Phys. Rev. Lett. **110**, 026103 (2013).
[21] B. Lavi and A. Marmur, Colloids Surf., A **250**, 409 (2004).
[22] A. Marmur and M. D. Lelah, Chem. Eng. Commun. **13**, 133 (1981).
[23] J. Lopez, C. A. Miller, and E. Ruckenstein, J. Colloid Interface Sci. **56**, 460 (1976).
[24] G. McHale, C. V. Brown, and N. Sampara, Nat. Commun. **4**, 1605 (2013).
[25] Q. Z. Yuan and Y. P. Zhao, J. Fluid Mech. **716**, 171 (2013).
[26] X. Y. Zhu, Q. Z. Yuan, and Y. P. Zhao, Sci. Rep. **2**, 927 (2012).
[27] T. Kajiya, A. Daerr, T. Narita, L. Royon, F. Lequeux, and L. Limat, Soft Matter **9**, 454 (2013).
[28] A. Eddi, K. G. Winkels, and J. H. Snoeijer, Phys. Fluids **25**, 013102 (2013).
[29] T. D. Blake, M. Bracke, and Y. D. Shikhmurzaev, Phys. Fluids **11**, 1995 (1999).
[30] T. D. Blake, A. Clarke, and K. J. Ruschak, AIChE J. **40**, 229 (1994).
[31] D. Beaglehole, J. Phys. Chem. **93**, 893 (1989).
[32] *Physical Properties of Glycerine and Its Solutions* (Glycerine Producers' Association, New York, 1963).
[33] D. Khossravi and K. A. Connors, J. Solution Chem. **22**, 321 (1993).

[34] J. B. Segur and H. E. Oberstar, Ind. Eng. Chem. **43**, 2117 (1951).
[35] Y. Nakamura, A. Carlson, G. Amberg, and J. Shiomi, Phys. Rev. E **88**, 033010 (2013).
[36] J. Eggers, J. R. Lister, and H. A. Stone, J. Fluid Mech. **401**, 293 (1999).
[37] J. D. Paulsen, J. C. Burton, and S. R. Nagel, Phys. Rev. Lett. **106**, 114501 (2011).
[38] D. Legendre and M. Maglio, Colloids Surf., A **432**, 29 (2013).
[39] A. Carlson, G. Bellani, and G. Amberg, Phys. Rev. E **85**, 045302(R) (2012).
[40] A. Carlson, M. Do-Quang, and G. Amberg, Phys. Fluids **21**, 121701 (2009).
[41] A. Carlson, M. Do-Quang, and G. Amberg, J. Fluid Mech. **682**, 213 (2011).
[42] H. Lamb, *Hydrodynamics* (Dover, New York, 1932).
[43] J. C. Baret, M. M. J. Decre, and F. Mugele, Langmuir **23**, 5173 (2007).